Electrocatalysis

International Edition: DOI: 10.1002/anie.201605551
German Edition: DOI: 10.1002/ange.201605551

Aligned MoO_x/MoS_2 Core–Shell Nanotubular Structures with a High Density of Reactive Sites Based on Self-Ordered Anodic Molybdenum Oxide Nanotubes

Bowen Jin, Xuemei Zhou, Li Huang, Markus Lickleder, Min Yang, and Patrik Schmuki**

Abstract: *The present work demonstrates the self-organized formation of anodic molybdenum oxide nanotube arrays. The amorphous tubes can be crystallized to MoO_2 or MoO_3 and be converted fully or partially into molybdenum sulfide. Vertically aligned MoO_x/MoS_2 nanotubes can be formed when, under optimized conditions, defined MoS_2 sheets form in a layer by layer arrangement that provide a high density of reactive stacking misalignments (defects). These core–shell nanotube arrays consist of a conductive suboxide core and a functional high defect density MoS_2 coating. Such structures are highly promising for applications in electrocatalysis (hydrogen evolution) or ion insertion devices.*

Molybdenum compounds, and particularly oxides and sulfides,[1] have for decades received attention owing to their unique chemical and physical properties and the resulting high potential not only in classic lubrication[2] but also for photochromic/ electrochromic devices,[3] photocatalysts,[4] high-energy-density supercapacitors,[5] lithium ion batteries,[6] and most recently as catalyst for electrochemical hydrogen generation.[1b,7] For many of these applications, the use of nanoscale geometries is highly advantageous owing to the high specific surface area and short carrier and ion diffusion pathways that can be established.[8] Among the various MoX materials, particularly MoS_2 is intensively investigated. This is to a large extent due to the weak van der Waals force between the stacked S-Mo-S units giving it a graphene-like layer structure.[9] This is not only the origin of outstanding lubrication properties but also the key to the insertion and extraction of small foreign ions into the free space of the S-Mo-S layers.[10]

In insertion devices the availability of layer edges plays a crucial role to provide access for ions to enter the galleys between the sheets. Layer edges also are regarded crucial for the remarkable electrocatalytic properties observed for MoS_2 for the promotion of the hydrogen evolution reaction (HER). The synthesis of defined MoS_2 nanostructures was pioneered more than 20 years ago by the finding of Tenne et al.[11] on the thermal synthesis of "onion-shell" MoS_2 structures. Meanwhile, various other synthesis paths for MoS_2-based nanomorphologies have been explored; these are mainly based on gas-phase reactions,[9–12] electrodeposition,[13] or wet-chemical template-assisted approaches.[14]

MoO_x and its 1D structures are generally found to be less effective to provide catalytic functionality and show generally lower ion insertion capacities, but the oxide and even more oxide/suboxide structures can provide a very high electron-conductivity.[15]

A particularly elegant combination of oxide and sulfide is thus the formation of core–shell structures (preferably vertically aligned to an electrode back contact) where the conductive oxide core (MoO_3/MoO_2) provides a charge transport pathway, and the MoS_2 shell enables above mentioned functionalities.[16] To date, the synthesis of defined 1D MoO_3/MoS_2 co-nanostructures has mainly been achieved by hydrothermal approaches[17] or catalyzed transport reactions.[18]

However, a most direct and facile approach to grow vertically aligned 1D MoO_x-nanotubular structures is self-ordering electrochemical anodization (SOA). Over the past ten years, SOA has been successfully developed and used to obtain highly ordered oxide nanotube or nanopore arrays on Al, Ti, W, Ta, Nb, Zr, Co, Fe and a variety of alloys.[19] Nevertheless, up to now there is no report on the successful fabrication of self-ordered molybdenum oxide nanoporous or nanotubular arrays. To achieve a self-ordered growth of an anodic oxide structure, a defined equilibrium needs to be established between anodic oxide formation and its dissolution[19b,20] However, Mo belongs to the class of metals where an optimized equilibrium is very hard to be experimentally established.[21]

Herein, we establish experimental conditions that enable the anodic growth of one-dimensional ordered molybdenum oxide nanotube arrays (Figure 1). These amorphous tubes can be converted into various crystalline oxide phases. Furthermore, we show that a partial conversion of these oxide tubes in H_2S can yield a unique oxide/sulfide core–shell structure where the conducting suboxide core is coated with conformal MoS_2 layers in a low angle, zig-zag configuration that provides a high density of stacking misalignments (Figure 1b). These structures show very promising first results in applications as an electrocatalyst for HER and as an anode in lithium ion battery configurations.

[*] B. Jin, L. Huang, Prof. Dr. M. Yang
MIIT Key Laboratory of Critical Materials Technology for New Energy Conversion and Storage, School of Chemistry and Chemical Engineering, Harbin Institute of Technology
Harbin, 150001 (PR China)
E-mail: yangmin@hit.edu.cn

X. Zhou, M. Lickleder, Prof. Dr. P. Schmuki
Department of Materials Science, Institute for Surface Science and Corrosion (LKO), University of Erlangen-Nuremberg
Martensstrasse 7, 91058 Erlangen (Germany)
E-mail: schmuki@ww.uni-erlangen.de

Supporting information for this article (including preparation and additional characterization results, for example, SEM, XRD) can be found under:
http://dx.doi.org/10.1002/anie.201605551.

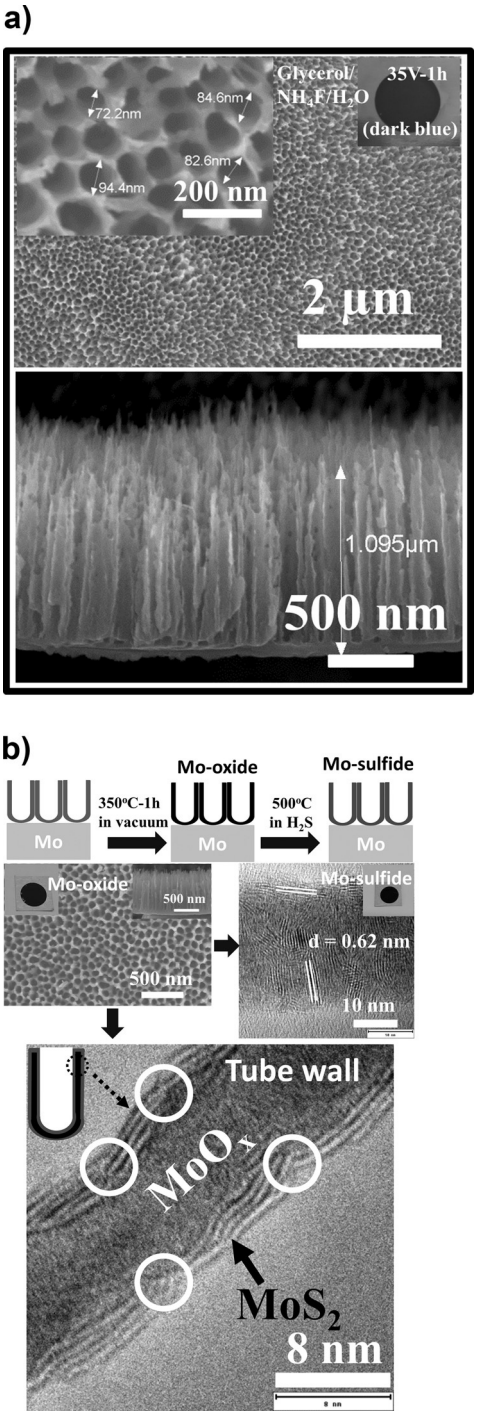

Figure 1. a) SEM images for top view and cross-section (inset: optical image) of the molybdenum oxide nanotubular structures anodized under optimized conditions (35 V for 1 h). b) Thermal conversion from as-formed molybdenum oxide to molybdenum sulfide. Upper row: SEM images for molybdenum oxide annealed at 350 °C for 1 h in vacuum; TEM image for full conversion into MoS_2 (annealed in H_2S at 500 °C for 30 min). Lower row: TEM image for partial conversion from molybdenum oxide to MoO_x/MoS_2 core–shell structure (annealed in H_2S at 500 °C for 2 min). Inset: position where this TEM image was taken from on the tube wall. The stacking misalignments of MoS_2 layers are marked in the white circles.

To achieve self-organized growth of Mo oxide structures, we explored a wide range of electrochemical conditions (an overview is given in the Supporting Information, Table S1).[19] We find that self-aligned organized oxide growth can be successfully and reliably established in fluoride-containing glycerol electrolytes; typical tube lengths for 1 h growth are 1 µm and the tube diameter can be controlled from 40 nm to 140 nm (Supporting Information, Figure S2 b). Figure 1 a gives an example of a self-ordered molybdenum oxide layer grown at 35 V for 1 h in the optimized electrolyte (0.4 M NH_4F in 10 vol. % H_2O/ 90 vol. % glycerol). Under these conditions, the nanotubes have a length of approximately 1 µm and an inner diameter of about 80 nm. The layers adhere very well to the substrate and exhibit long range order, that is, coat uniformly the entire anodized surface.

XRD of the nanotube layers shows the as-grown tubes to be amorphous (Figure 2 d), and XPS in Figure 2 suggests the tube composition of these as-formed samples to be close to a MoO_3 stoichiometry.

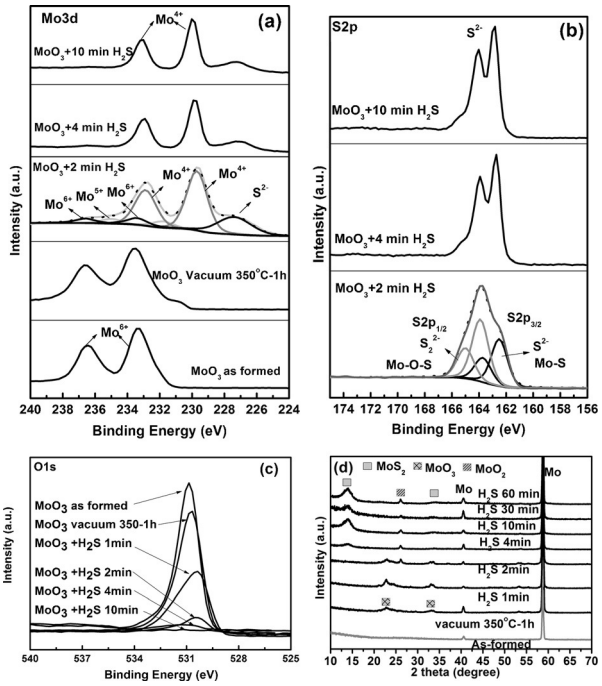

Figure 2. XPS spectra of a) Mo 3d, b) S 2p, c) and O 1s peaks of the samples before and after sulfurization in H_2S for MoO_3 annealed in vacuum at 350 °C for 1 h. d) XRD patterns of MoO_3 nanotube layers after sulfurization.

To convert the amorphous layers into a defined crystallinity, samples were annealed under various conditions (250 °C, 350 °C, 450 °C in air and vacuum, respectively). XRD and SEM data of samples after the annealing experiments are shown in the Supporting Information, Figures S4–S6. The results demonstrate that a variety of amorphous and crystalline tubes can be produced using different thermal treatments. In this work we selected annealing in vacuum for further work as these tubes were found to be the most suitable for an optimized conversion to a MoO_x/MoS_2 core–shell

structure. The corresponding XRD spectra (Supporting Information, Figure S4) reveal that upon annealing up to 250 °C, the XRD pattern remains the same as for the as-prepared amorphous molybdenum oxide layer; for higher temperature one finds the formation of a desired mixed stoichiometry of MoO_2 and MoO_3. This is not only evident in XRD (Figure 2 d) but also from XPS (Figure 2 a) where the Mo peak in XPS for samples after vacuum annealing exhibits a shoulder at lower binding energy, which shows that some of the Mo remains reduced after the vacuum treatment[22] (as described in more detail in the Supporting Information). The most defined and stable crystalline conditions are provided by vacuum annealing at 350 °C. Under these conditions not only crystallinity but also the morphology of the nanotubes is maintained (optical and SEM images in Figure 1 b, and XRD patterns in Figure 2), while higher temperatures lead to a thermal sintering of the structures (Supporting Information, Figures S5, S6).

These oxide tubes provide the basis for the formation of MoO_x/MoS_2 core–shell structures; this by a partial sulfurization, as shown in Figure 1 b. Various annealing treatments in H_2S at different temperatures and durations were examined and the nanotubes then characterized in view of morphology, structure, and composition (as described in more detail in the Supporting Information). The effect of the H_2S treatment on the oxide can be well followed by XRD and XPS. Examples for a treatment of the tube layers in H_2S at 500 °C for various exposure times are shown in Figure 2 and the Supporting Information, Figure S7. With increasing sulfurization time, XRD and XPS spectra show a gradual conversion from oxide into sulfide. From XRD for sulfurization for more than 2 min, a clear peak at $2\theta = 14.3°$ assigned to MoS_2 is observed. With prolonged treatment (60 min), there is an increase of the peak intensity of MoS_2, while the MoO_3 peaks disappear, and gradually the formation of MoO_2 peaks at 26.0° can be observed. This shows that with increasing H_2S treatment time, besides sulfide formation, also a partial reduction of MoO_3 to MoO_2 takes place.

Figure 2 b shows XPS spectra for a sample treated for 2 min in H_2S. The S 2p region indicates that at least two chemical states of S overlap. The doublet at 165.0 eV and 163.9 eV is assigned to S in a Mo-O-S configuration, the doublet of 163.8 eV and 162.5 eV to Mo-S bands, respectively.[23] After annealing in H_2S for 4 min and 10 min the latter regime increases,[24] consistent with the formation of additional MoS_2 with extended sulfurization time, the peak intensity of O1s decreases gradually, in line with above XRD data and EDX measurements (Supporting Information, Table S2).

SEM images taken after sulfurization (Figure 1 b; Supporting Information, Figure S7) show that layer thickness and tube diameter are maintained after the H_2S treatment, however a slight roughening of the tube walls can be observed.

TEM for samples exposed to H_2S for extended times (for example, 30 min in Figure 1 b) show a full conversion of the oxide walls to MoS_2. For H_2S treatment times of 10 s to 2 min nanotube walls with core–shell structures can be produced. The TEM image (Figure 1 b, lower; Supporting Information, Figure S8) shows a tube wall of a sample treated for 2 min where four distinct layers of MoS_2 have been formed on the outer tube wall. The layers are present conformally over the tube with layers grown with an offset of 10°–15° to the tube normal leading to a zig-zag arrangement of the MoS_2-sheets, and bent MoS_2 nanosheets consisting of stacks of typically four S-Mo-S layer units, which are discordantly grown on the MoO_x substrate, exposing catalytically active end planes to the surrounding. These stacking misalignments in the MoS_2 layers repeat approximately every 6 nm. XPS confirms the presence of MoS_2 (Figure 2 a) with Mo^{4+} located at a lower binding energy (232.8 eV and 229.6 eV) and a sole peak at 227.4 eV corresponding to S^{2-}.[25] Moreover, Mo^{6+} and Mo^{5+} peaks are still visible in the spectra, confirming the core to still consist of a mixed phase of MoO_3 and MoO_2 (in line with XRD; Figure 2 d).

To explore the potential value of the core–shell structures we tested the tubes for their performance as an electrocatalytic HER evolution catalyst and carried out some preliminary experiments regarding the potential use as an anode in a Li-insertion battery configuration. Hydrogen evolution reaction (HER) measurements were carried out, as described in the Supporting Information. Figure 3 a shows

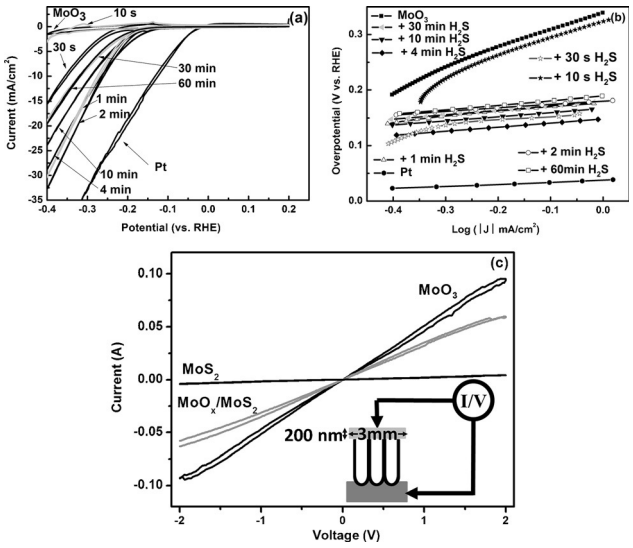

Figure 3. a) Polarization curves for self-ordered MoO_3 nanoporous layers under various sulfurization time (10 s, 30 s, 1 min, 2 min, 4 min, 10 min, 30 min, and 60 min, respectively), in comparison with a Pt sheet sample. Potential window is −0.4 to 0.2 V (vs. RHE) with scan rate of 5 $mV s^{-1}$. b) Tafel analysis of the data presented in (a). c) Solid-state *I–V* measurements for MoO_3 annealed at 350 °C for 1 h in vacuum, MoO_x/MoS_2 and MoS_2 nanotube layers. Inset: illustrations for the molybdenum oxide NT layers used for the *I–V* measurements.

polarization curves of the anodic MoO_3 annealed for various heat-treatment conditions (in vacuum and in H_2S) in comparison with a Pt sheet. The onset potentials of all self-ordered MoO_x/MoS_2 nanotube arrays are at approx. −110 mV to −160 mV vs. RHE. The pure MoO_3 layers show only a very low activity, whereas the sulfurized samples (from 30 s to 60 min) show significantly higher current densities at com-

parably low overpotentials. A comparison of the potential required to generate a current density of $10\,mA\,cm^{-2}$ is illustrated in the Supporting Information, Table S3. Among these samples, clearly the samples after 2 min-sulfurization (that is, the core–shell structure in Figure 1b) show the highest HER activity with a current density of $-16\,mA\,cm^{-2}$ at -300 mV vs. RHE ($-10\,mA\,cm^{-2}$ at -259 mV vs. RHE). Samples that were treated for longer times in H_2S exhibit a significant decrease in the HER activity (Figure 3a). The highest Tafel slope we obtained was $63\,mV\,dec^{-1}$ for MoO_x/MoS_2 core–shell structure sample. Tafel plots are shown in Figure 3b where the slope reflects the electrochemical resistance for H_2 generation. A comparison with literature data (Supporting Information, Table S3) demonstrates the beneficial effect of the core–shell structure. To test if this is due to the desired combination of MoS_2 functionality with oxide conductivity, we acquired solid-state *I–V* curves (Figure 3c). Indeed we find the conductivity of the core–shell structure (30.91 Ω) to be very similar to a reduced MoO_3 tube layer (21.03 Ω) while the tube layers converted to MoS_2 for longer times show a significantly higher resistivity (471.71 Ω). This shows that the synergy between core and shell operates well. Moreover, previous reports have shown that the edges of the two-dimensional MoS_2 catalysts are active sites for the HER reactions, especially when these basal planes are oriented off-axis to the sample surface.[1b,7a] Hence the presence of the high number of stacking misalignments in the MoS_2 layers enhances the number of active sites for HER reactions. However, usually disorder, such as stacking misalignments, are reported to be highly detrimental to the intrinsic conductivity of MoS_2. Therefore the underlying conductive MoO_x core (with a short carrier transport paths in MoS_2) is particularly important. It is also noteworthy that, in this case, the outside shell of MoS_2 not only provides active sites for HER activity but also provides the electrode stability against corrosion (Supporting Information, Figures S9–S11), and in line with previous reports[16] (see also further experiments in the Supporting Information).

While recently other very promising sulfide or phosphide compounds have been reported,[26] the key of the present work is that it shows the direct facile formation of a MoO_x/MoS_2 core–shell structure (nanotube arrays) that is directly back contacted, and thus can directly be used as an electrode. Moreover, it is noteworthy that even in the present state of optimization (Supporting Information, Figure S12), a slightly better performance can be achieved than any previous reported core–shell MoO_3/MoS_2 nanostructure.[16]

As mentioned, the here synthesized core–shell structures are also of interest for lithium insertion devices,[6] as a key issue in MoS_2 based battery devices is to combine the high lithium intercalation capacity of MoS_2 with conductivity (commonly addressed by using MoS_2/graphitic carbon composites). Some preliminary data for the use of our 1D MoO_x/MoS_2 core–shell structures as an anode for lithium intercalation is given in the Supporting Information, Figure S13. First data show an initial specific capacity for the core–shell structure to be in the range of 620 to $846\,mA\,h\,g^{-1}$ at $0.1\,mA\,cm^{-2}$. This is, in comparison with other reported data, a very promising result (Supporting Information, Table S4). This aspect will be followed up in detail in further work.

In summary, we show for the first time the successful synthesis of anodic self-organized MoO_3 nanotube layers. These layers could be used in classical applications of molybdenum oxides such as solid-state lithium batteries, gas sensors, and electrochromic materials. The oxide nanotubular layer, however, can be further converted by sulfurization to MoO_x/MoS_2 core–shell nanotube structures. The high density of regular stacking misalignments in the outer MoS_2 sheets providing a high number of exposed reactive sites is remarkable. These MoO_x/MoS_2 core–shell structures thus exhibit an effective synergy between conductivity and reactivity that is evident from a high hydrogen evolution electrocatalytic activity that furthermore provides a promising platform for wider electrochemical and photoelectrochemical applications.

Acknowledgements

The authors thank Nhat Truong Nguyen for TEM, Gihoon Cha for the battery tests, Dr. Harald Gunselmann and Dr. Ringel Lorenz for the H_2S detection, and Imgon Hwang for the solid-state *I–V* measurements. This work is financially supported by the National Natural Science Foundation of China (No. 21203043), China Postdoctoral Science Foundation (No. 2012M520729 and No. 2013T60361), ERC, DFG, DFG-funcos and the DFG Cluster of Excellence EAM.

Keywords: anodization · core–shell structures · H_2 evolution · molybdenum oxide · nanotubes

How to cite: *Angew. Chem. Int. Ed.* **2016**, *55*, 12252–12256
Angew. Chem. **2016**, *128*, 12440–12444

[1] a) Y. Yan, B. Y. Xia, Z. Xu, X. Wang, *ACS Catal.* **2014**, *4*, 1693–1705; b) J. D. Benck, T. R. Hellstern, J. Kibsgaard, P. Chakthranont, T. F. Jaramillo, *ACS Catal.* **2014**, *4*, 3957–3971; c) X. Huang, Z. Zeng, H. Zhang, *Chem. Soc. Rev.* **2013**, *42*, 1934–1946; d) X. Hu, W. Zhang, X. Liu, Y. Mei, Y. Huang, *Chem. Soc. Rev.* **2015**, *44*, 2376–2404.

[2] a) R. Holinski, J. Gansheim, *Wear* **1972**, *19*, 329–342; b) W. O. Winer, *Wear* **1967**, *10*, 422–452; c) L. Rapoport, Y. Bilik, Y. Feldman, M. Homyonfer, S. R. Cohen, R. Tenne, *Nature* **1997**, *387*, 791–793.

[3] a) C. G. Granqvist, *Handbook of Inorganic Electrochromic Materials*, Elsevier, Amsterdam, **1995**; b) P. M. S. Monk, R. J. Mortimer, D. R. Rosseinsky, *Electrochromism and Electrochromic Devices*, Cambridge University Press, Cambridge, **2007**; c) S. K. Deb, J. A. Chopoorian, *J. Appl. Phys.* **1966**, *37*, 4818–4825.

[4] a) H. Tributsch, J. C. Bennett, *I. J. Electroanal. Chem.* **1977**, *81*, 97–111; b) W. Zhou, Z. Yin, Y. Du, X. Huang, Z. Zeng, Z. Fan, H. Liu, J. Wang, H. Zhang, *Small* **2013**, *9*, 140–147; c) E. Parzinger, B. Miller, B. Blaschke, J. A. Garrido, J. W. Ager, A. Holleitner, U. Wurstbauer, *ACS Nano* **2015**, *9*, 11302–11309.

[5] a) M. Acerce, D. Voiry, M. Chhowalla, *Nat. Nanotechnol.* **2015**, *10*, 313–318; b) B. Mendoza-Sánchez, T. Brousse, C. Ramirez-Castro, V. Nicolosi, P. S. Grant, *Electrochim. Acta* **2013**, *91*, 253–260; c) W. Tang, L. Liu, S. Tian, L. Li, Y. Yue, Y. Wu, K. Zhu, *Chem. Commun.* **2011**, *47*, 10058–10060.

[6] a) R. R. Haering, J. A. R. Stiles, K. Brandt, US Patent 4224390, **1980**; b) C. Q. Feng, J. Ma, H. Li, R. Zeng, Z. P. Guo, H. K. Liu, *Mater. Res. Bull.* **2009**, *44*, 1811 – 1815; c) Y. Cheng, A. Nie, Q. Zhang, L.-Y. Gan, R. Shahbazian-Yassar, U. Schwingenschlogl, *ACS Nano* **2014**, *8*, 11447 – 11453; d) T. Stephenson, Z. Li, B. Olsen, D. Mitlin, *Energy Environ. Sci.* **2014**, *7*, 209 – 231.

[7] a) T. F. Jaramillo, K. P. Jørgensen, J. Bonde, J. H. Nielsen, S. Horch, I. Chorkendorff, *Science* **2007**, *317*, 100 – 102; b) D. Merki, X. L. Hu, *Energy Environ. Sci.* **2011**, *4*, 3878 – 3888; c) H. T. Wang, Z. Y. Lu, D. S. Kong, J. Sun, T. M. Hymel, Y. Cui, *ACS Nano* **2014**, *8*, 4940 – 4947.

[8] a) H. I. Karunadasa, E. Montalvo, Y. Sun, M. Majda, J. R. Long, C. J. Chang, *Science* **2012**, *335*, 698 – 702; b) T. Wang, L. Liu, Z. Zhu, P. Papakonstantinou, J. Hu, H. Liu, M. Li, *Energy Environ. Sci.* **2013**, *6*, 625 – 633; c) J. Kibsgaard, Z. Chen, B. N. Reinecke, T. F. Jaramillo, *Nat. Mater.* **2012**, *11*, 963 – 969.

[9] a) Y. Feldman, E. Wasserman, D. J. Srolovitz, R. Tenne, *Science* **1995**, *267*, 222 – 225; b) R. Tenne, *Nat. Nanotechnol.* **2006**, *1*, 103 – 111.

[10] Q. H. Wang, K. Kalantar-Zadeh, A. Kis, J. N. Coleman, M. S. Strano, *Nat. Nanotechnol.* **2012**, *7*, 699 – 712.

[11] L. Margulis, G. Salitra, R. Tenne, M. Talianker, *Nature* **1993**, *365*, 113 – 114.

[12] a) M. Hershfinkel, L. A. Gheber, V. Volterra, J. L. Hutchison, L. Margulis, R. Tenne, *J. Am. Chem. Soc.* **1994**, *116*, 1914 – 1917; b) D. J. Srolovitz, S. A. Safran, M. Homyonfer, R. Tenne, *Phys. Rev. Lett.* **1995**, *74*, 1779 – 1782.

[13] D. Merki, S. Fierro, H. Vrubel, X. Hu, *Chem. Sci.* **2011**, *2*, 1262 – 1267.

[14] a) J. Kibsgaard, T. F. Jaramillo, F. Besenbacher, *Nat. Chem.* **2014**, *6*, 248 – 253; b) Y. D. Hou, B. L. Abrams, P. C. K. Vesborg, M. E. Bjorketun, K. Herbst, L. Bech, A. M. Setti, C. D. Damsgaard, T. Pedersen, O. Hansen, J. Rossmeisl, S. Dahl, J. K. Norskov, I. Chorkendorff, *Nat. Mater.* **2011**, *10*, 434 – 438; c) J. D. Benck, Z. Chen, L. Y. Kuritzky, A. J. Forman, T. F. Jaramillo, *ACS Catal.* **2012**, *2*, 1916 – 1923; d) C. R. Germán, P. Santiago, J. A. Ascencio, U. Pal, M. Pérez-Alvarez, L. Rendón, D. Mendoza, *J. Phys. Chem. B* **2005**, *109*, 17488 – 17495.

[15] a) M. A. K. L. Dissanayake, L. L. Chase, *Phys. Rev. B* **1978**, *18*, 6872 – 6879; b) V. Bhosle, A. Tiwari, J. Narayan, *J. Appl. Phys.* **2005**, *97*, 083539.

[16] Z. Chen, D. Cummins, B. N. Reinecke, E. Clark, M. K. Sunkara, T. F. Jaramillo, *Nano Lett.* **2011**, *11*, 4168 – 4175.

[17] J. Chen, N. Kuriyama, H. Yuan, H. T. Takeshita, T. Sakai, *J. Am. Chem. Soc.* **2001**, *123*, 11813 – 11814.

[18] M. Remskar, A. Mrzel, Z. Skraba, A. Jesih, M. Ceh, J. Demsÿar, P. Stadelmann, F. Levy, D. Mihailovic, *Science* **2001**, *292*, 479 – 481.

[19] a) K. Lee, A. Mazare, P. Schmuki, *Chem. Rev.* **2014**, *114*, 9385 – 9454; b) P. Roy, S. Berger, P. Schmuki, *Angew. Chem. Int. Ed.* **2011**, *50*, 2904 – 2939; *Angew. Chem.* **2011**, *123*, 2956 – 2995; c) H. Masuda, K. Fukuda, *Science* **1995**, *268*, 1466 – 1468; d) V. Zwilling, E. Darque-Ceretti, A. Boutry-Forveille, D. David, M. Y. Perrin, M. Aucouturier, *Surf. Interface Anal.* **1999**, *27*, 629 – 637.

[20] a) V. P. Parkhutik, V. I. Shershulsky, *J. Phys. D* **1992**, *25*, 1258 – 1263; b) K. R. Hebert, S. P. Albu, I. Paramasivam, P. Schmuki, *Nat. Mater.* **2012**, *11*, 162 – 166.

[21] a) M. R. Arona, R. Kelly, *J. Electrochem. Soc.* **1972**, *119*, 270; b) S. Ikonopisov, *Electrodeposition Surf. Treat.* **1974**, *2*, 411 – 418; c) M. Pourbaix, *Atlas of Electrochemical Equilibria in Aqueous Solutions 2nd Edition*, National Association of Corrosion Engineers, **1974**.

[22] W. E. Swartz, D. M. Hercules, *Anal. Chem.* **1971**, *43*, 1774 – 1779.

[23] a) L. Benoist, D. Gonbeau, G. P. Guillouzo, E. Schmidt, G. Meunier, A. Levasseur, *Thin Solid Films* **1995**, *258*, 110 – 114; b) G. C. Stevens, T. Edmonds, *J. Catal.* **1975**, *37*, 544 – 547.

[24] J. R. Lince, D. J. Carre, P. D. Fleischauer, *Langmuir* **1986**, *2*, 805 – 808.

[25] N. H. Turner, A. M. Single, *Surf. Interface Anal.* **1990**, *15*, 215 – 222.

[26] a) M. Cabán-Acevedo, M. L. Stone, J. R. Schmidt, J. G. Thomas, Q. Ding, H.-C. Chang, M.-L. Tsai, J.-H. He, S. Jin, *Nat. Mater.* **2015**, *14*, 1245 – 1251; b) J. Tian, Q. Liu, N. Cheng, A. M. Asiri, X. Sun, *Angew. Chem. Int. Ed.* **2014**, *53*, 9577 – 9581; *Angew. Chem.* **2014**, *126*, 9731 – 9735; c) E. J. Popczun, C. G. Read, C. W. Roske, N. S. Lewis, R. E. Schaak, *Angew. Chem. Int. Ed.* **2014**, *53*, 5427 – 5430; *Angew. Chem.* **2014**, *126*, 5531 – 5534; d) J. Kibsgaard, T. F. Jaramillo, *Angew. Chem. Int. Ed.* **2014**, *53*, 14433 – 14437; *Angew. Chem.* **2014**, *126*, 14661 – 14665.

Received: June 7, 2016
Published online: September 7, 2016

